Human Molecular Genetics, 2015, Vol. 24, No. 7 1813–1823

doi: 10.1093/hmg/ddu595
Advance Access Publication Date: 28 November 2014
Original Article

ORIGINAL ARTICLE

Fragile X-like behaviors and abnormal cortical dendritic spines in *Cytoplasmic FMR1-interacting protein 2*-mutant mice

Kihoon Han[1,2,6,*], Hogmei Chen[3,5,6], Vincenzo A. Gennarino[1,6], Ronald Richman[1,2,6], Hui-Chen Lu[3,4,5,6], and Huda Y. Zoghbi[1,2,3,4,6,*]

[1]Department of Molecular and Human Genetics, [2]The Howard Hughes Medical Institute, [3]Departments of Pediatrics and, [4]Program in Developmental Biology and Department of Neuroscience, Baylor College of Medicine, Houston, TX 77030, USA, [5]The Cain Foundation Laboratories, and [6]Jan and Dan Duncan Neurological Research Institute, Texas Children's Hospital, Houston, TX 77030, USA

*To whom correspondence should be addressed at: Neurological Research Institute at Texas Children's Hospital, Houston, TX 77030, USA. Tel: +1 7137986558; Fax: +1 7137988728; Email: kihoonh@bcm.edu (K.H.) or hzoghbi@bcm.edu (H.Y.Z.)

Abstract

Silencing of fragile X mental retardation 1 (*FMR1*) gene and loss of fragile X mental retardation protein (FMRP) cause fragile X syndrome (FXS), a genetic disorder characterized by intellectual disability and autistic behaviors. FMRP is an mRNA-binding protein regulating neuronal translation of target mRNAs. Abnormalities in actin-rich dendritic spines are major neuronal features in FXS, but the molecular mechanism and identity of FMRP targets mediating this phenotype remain largely unknown. Cytoplasmic FMR1-interacting protein 2 (Cyfip2) was identified as an interactor of FMRP, and its mRNA is a highly ranked FMRP target in mouse brain. Importantly, Cyfip2 is a component of WAVE regulatory complex, a key regulator of actin cytoskeleton, suggesting that Cyfip2 could be implicated in the dendritic spine phenotype of FXS. Here, we generated and characterized *Cyfip2*-mutant ($Cyfip2^{+/-}$) mice. We found that $Cyfip2^{+/-}$ mice exhibited behavioral phenotypes similar to *Fmr1*-null ($Fmr1^{-/y}$) mice, an animal model of FXS. Synaptic plasticity and dendritic spines were normal in $Cyfip2^{+/-}$ hippocampus. However, dendritic spines were altered in $Cyfip2^{+/-}$ cortex, and the dendritic spine phenotype of $Fmr1^{-/y}$ cortex was aggravated in $Fmr1^{-/y}$; $Cyfip2^{+/-}$ double-mutant mice. In addition to the spine changes at basal state, metabotropic glutamate receptor (mGluR)-induced dendritic spine regulation was impaired in both $Fmr1^{-/y}$ and $Cyfip2^{+/-}$ cortical neurons. Mechanistically, mGluR activation induced mRNA translation-dependent increase of Cyfip2 in wild-type cortical neurons, but not in $Fmr1^{-/y}$ or $Cyfip2^{+/-}$ neurons. These results suggest that misregulation of Cyfip2 function and its mGluR-induced expression contribute to the neurobehavioral phenotypes of FXS.

Introduction

Fragile X syndrome (FXS) is the most common inherited cause of intellectual disability, accompanied by additional symptoms including autistic behaviors, increased susceptibility to seizures, craniofacial abnormalities and macroorchidism (1,2). The majority of FXS is caused by the expansion of CGG trinucleotide repeats (>200) in the 5′ untranslated region of fragile X mental retardation 1 (*FMR1*) gene, which in turn results in transcriptional silencing of the gene and loss of fragile X mental retardation protein (FMRP) (3–6). FMRP is a polyribosome-associated mRNA-binding protein that is highly abundant in neurons and is involved in regulating the transport and translation of hundreds of target mRNAs (2,7).

Received: September 9, 2014. **Revised:** October 30, 2014. **Accepted:** November 24, 2014

© The Author 2014. Published by Oxford University Press. All rights reserved. For Permissions, please email: journals.permissions@oup.com

Downloaded from https://academic.oup.com/hmg/article-abstract/24/7/1813/595301
by guest
on 14 March 2018

Therefore, loss of regulation of target mRNAs is considered as the core molecular pathophysiology of FXS (7).

Several forms of neuronal synaptic plasticity and function are altered in the mouse model of FXS (1). Specifically, group 1 metabotropic glutamate receptor (mGluR1 and mGluR5)-dependent long-term depression (LTD) is enhanced and no longer requires new protein synthesis in the hippocampus of *Fmr1*-null mice (8,9). Moreover, genetic or pharmacological inhibition of mGluR in animal models of FXS rescues many of the FXS-related phenotypes (1,10). Increased number of immature dendritic spines is also observed in the brains of *Fmr1*-null mice as well as FXS patients (11,12). The actin cytoskeleton is the structural basis of dendritic spines and is regulated by Rho family of small GTPases such as Cdc42, Rac1 and RhoA (13,14). FMRP has been associated with Rac1 signaling either by directly interacting with the protein components [p21-activated kinase (PAK) and Cytoplasmic FMR1-interacting protein] or by regulating their mRNA translation (15–18). Furthermore, genetic or pharmacological inhibition of PAK, a downstream effector of Rac1, rescues the dendritic spine phenotype and some of FXS-related behaviors in *Fmr1*-null mice (18,19). These results suggest that, together with enhanced mGluR signaling, abnormal regulation of the actin cytoskeleton could underlie the neuropathogenesis of FXS. However, the molecular mechanism and the identity of FMRP target proteins involved in the regulation of actin cytoskeleton and dendritic spines in FXS remain largely unknown.

Cytoplasmic FMR1-interacting protein 1 and 2 (Cyfip1/2, also called Sra1 and Pir121, respectively) were identified as direct binding partners of FMRP in yeast two-hybrid screening (20). The most well-characterized function of Cyfip is as a component of ~400-kDa heteropentameric WAVE regulatory complex (WRC), consisting of WAVE/SCAR, Cyfip, Nap/Hem/Kette, Abi and HSPC300/Brick, which activates Arp2/3 complex to initiate actin polymerization and branching (21). During basal condition, Cyfip inhibits WAVE activity of WRC by sequestering the activity-bearing VCA domain of WAVE (22). However, binding of an upstream regulator Rac1-GTP to Cyfip induces conformational change and subsequent release of the VCA domain to activate Arp2/3 complex (22). In addition, Cyfip is important for the stability of WAVE (23). Because of this dual role of Cyfip, it is not easy to decipher the net effect of loss of Cyfip on actin assembly. Interestingly, in *Cyfip*-null *Drosophila*, the filamentous actin assembly is enhanced in spite of reduced WAVE protein level, suggesting that, without Cyfip, WAVE is first activated and then degraded (24).

Several studies showed functional relationship between Cyfip and FMRP (25). First, Cyfip1 was proposed to be an initiation factor 4E-binding protein that, together with FMRP, represses cap-dependent translational initiation (26). Second, a recent report showed that *Cyfip1* haploinsufficient mice have enhanced, and protein synthesis-independent, mGluR-LTD, similar to *Fmr1*-null mice (27). In contrast to Cyfip1, however, Cyfip2 is much less characterized in terms of its functional relationship to FMRP. Notably, *Cyfip2* mRNA was ranked as the ninth FMRP target among 842 FMRP-interacting brain polyribosomal mRNAs, whereas *Cyfip1* mRNA was not identified in the same study (28). Moreover, Cyfip2, but not Cyfip1, protein level is increased in the FXS lymphocytes (29). These results suggest that FMRP could directly regulate expression of Cyfip2, but not Cyfip1, and that Cyfip1 and Cyfip2 could have differential neuronal functions. To answer these questions, we generated *Cyfip2* heterozygous (*Cyfip2*$^{+/-}$) mice and, in parallel with *Fmr1*-null mice, characterized their behavioral phenotypes, biochemical, cellular and electrophysiological changes in brain. Here, we provide evidence for the role of Cyfip2 in fragile X-like behaviors and regulation of dendritic spines, and for the mGluR-induced regulation of Cyfip2 expression, which could provide new insight into the pathogenesis of the neurological FXS phenotypes.

Results

Expression analysis of Cyfip2 and its interacting proteins in *Cyfip2*$^{+/-}$ mice

We generated *Cyfip2*-mutant mice using the embryonic stem (ES) cells where the N-terminal exons (2 to 15) of *Cyfip2* gene were replaced with a *lacZ* cassette. However, we found that *Cyfip2* homozygous null mice were lethal before weaning age (postnatal day 21), consistent with a recent report where they observed perinatal lethality of *Cyfip2*-null mice generated with different *Cyfip2*-targeted ES cells (30). Therefore, in this study, we explored the roles of Cyfip2 in brain function using *Cyfip2* heterozygous (*Cyfip2*$^{+/-}$) mice that were viable with no overt phenotype. First, we investigated the brain regional expression pattern of *Cyfip2* using the *lacZ* cassette of *Cyfip2* ES cell. The X-gal staining of brain slices from 8-week-old *Cyfip2*$^{+/-}$ mice showed signals in various regions including the outer layers of cortex, hippocampus and striatum (Fig. 1A). In cerebellum, the signal was also detected in Purkinje cells. The overall brain cytoarchitecture of *Cyfip2*$^{+/-}$ mice was normal (Fig. 1B). We also performed quantitative real-time reverse transcription PCR (qRT-PCR) to measure the expression of *Cyfip1*, *Cyfip2* and *Wave-1* mRNAs in cortex, striatum, hippocampus and cerebellum of 10-week-old wild-type (WT) mice. We found that all three mRNAs were most abundant in cortex followed by striatum and hippocampus, and least expressed in cerebellum (Fig. 1C). Consistent with the mRNA expression pattern, endogenous Cyfip2 and WAVE proteins were detected in various brain regions with enrichment in the cortex and striatum (Fig. 1D). In subcellular fractions, Cyfip2 was detected in both soluble cytosol (S2) and synaptic fraction (PSDI), whereas WAVE was more localized in synaptic fractions (P2 and PSDI) (Fig. 1D).

In *Cyfip2*$^{+/-}$ hippocampus and cortex, *Cyfip2* mRNA levels were decreased by ~50%, but expression levels of *Cyfip1* and *Wave-1* mRNAs were not significantly changed (Fig. 1E). Hippocampal and cortical Cyfip2 protein levels were decreased to 50 and 70% of WT levels, respectively, in synaptosome of *Cyfip2*$^{+/-}$ mice (Fig. 1F). Consistent with the role of Cyfip in WAVE stability (23), WAVE protein level was also decreased in cortex, but not in hippocampus of *Cyfip2*$^{+/-}$ mice (Fig. 1F). This region-specific decrease of WAVE was not due to compensatory increase of Cyfip1 in hippocampus, as Cyfip1 levels were normal in both brain regions of *Cyfip2*$^{+/-}$ mice (Fig. 1F). It might suggest that WAVE stability is more dependent on Cyfip2 in cortex.

Cyfip2$^{+/-}$ mice exhibit fragile X-like behaviors

Next, we investigated behavioral phenotypes of *Cyfip2*$^{+/-}$ mice. We crossed male *Cyfip2*$^{+/-}$ mice with female *Fmr1*$^{+/-}$ mice to obtain male littermates with four genotypic combinations (WT, *Fmr1*$^{-/y}$ [null], *Cyfip2*$^{+/-}$ and *Fmr1*$^{-/y}$;*Cyfip2*$^{+/-}$ [double mutant]). This made it possible to test the behaviors of *Cyfip2*$^{+/-}$ mice in parallel with *Fmr1*$^{-/y}$ mice, and any genetic interaction (rescue or synergy) between them. The behavioral phenotypes of *Fmr1*$^{-/y}$ mice have been extensively characterized in various genetic backgrounds (31). We chose the following behavioral assays to examine our mice because *Fmr1*$^{-/y}$ mice showed consistent changes in these tests.

Downloaded from https://academic.oup.com/hmg/article-abstract/24/7/1813/595301
by guest
on 14 March 2018

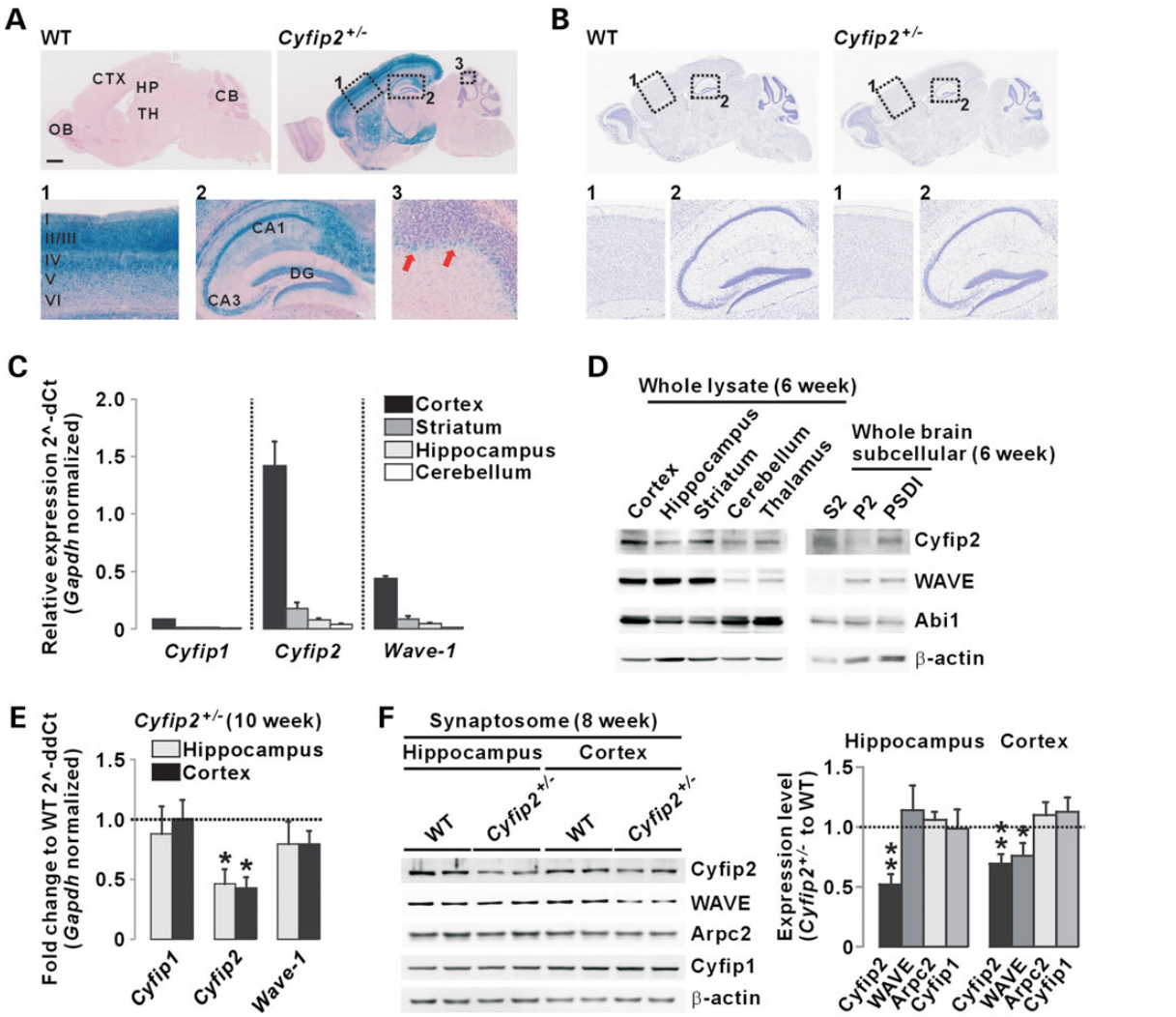

Figure 1. Expression analysis of Cyfip2 and its interacting proteins in *Cyfip2*$^{+/-}$ mice. (**A**) X-gal staining of *Cyfip2*$^{+/-}$ brain shows signals in various regions including cortex (Box 1), striatum, hippocampus (Box 2) and cerebellum (Box 3). The red arrows indicate Purkinje cells. There is no signal in WT brain. Scale bar 1 mm. CB, cerebellum; CTX, cortex; DG; dentate gyrus; HP, hippocampus; OB olfactory bulb; TH, thalamus. (**B**) Cresyl violet staining shows normal brain cytoarchitecture of *Cyfip2*$^{+/-}$ mice. (**C**) qRT-PCR analysis of *Cyfip1*, *Cyfip2* and *Wave-1* mRNA expression in WT brain regions. (**D**) Western blots show brain regional and subcellular expression patterns of Cyfip2, WAVE and Abi1. S2, soluble cytosol; P2, crude synaptosome; PSDI, Triton X-100 extract from P2. (**E**) qRT-PCR analysis shows expression changes of *Cyfip1*, *Cyfip2* and *Wave-1* mRNAs in *Cyfip2*$^{+/-}$ hippocampus and cortex compared with WT mice. (**F**) Representative western blots and quantification show expression changes of Cyfip2 and its interacting proteins in hippocampal and cortical synaptosome of *Cyfip2*$^{+/-}$ mice compared with WT mice ($n = 7$ animals per genotype). Arpc2 is a subunit of Arp2/3 complex. $^{*}P < 0.05$, $^{**}P < 0.01$. Statistical analyses for western blot assays are in Supplementary Material, Table S1.

In the open-field test, *Fmr1*$^{-/y}$ mice displayed increased locomotor activity (Fig. 2A and B), as reported previously (31). Interestingly, *Cyfip2*$^{+/-}$ mice were also hyperactive compared with WT mice (Fig. 2A and B). Notably, in double-mutant mice, the hyperactivity was significantly aggravated compared with *Fmr1*$^{-/y}$ mice (Fig. 2A). Center-to-total distance ratio and vertical activity count during the open-field test were similar in all genotypes (Fig. 2C and D). For the stereotypy count during the open-field test, only double-mutant mice showed significant increase compared with WT mice (Fig. 2E). In the light–dark box assay, measuring anxiety-like behavior, both *Fmr1*$^{-/y}$ and *Cyfip2*$^{+/-}$ mice displayed increased transitions between light and dark areas (Fig. 2F). In double-mutant mice, this phenotype was significantly enhanced (Fig. 2F). Furthermore, only double-mutant mice spent significantly more time in the light area compared with WT mice (Fig. 2G). In the test of auditory sensory processing, *Fmr1*$^{-/y}$, *Cyfip2*$^{+/-}$ and double-mutant mice commonly showed decreased startle response and enhanced prepulse inhibition (Fig. 2H and I). Finally, we tested nociception using hot plate and found that only *Fmr1*$^{-/y}$ mice showed delayed response compared with WT mice (Fig. 2J). The body weights were not significantly different among all genotypes at 11 weeks old (Fig. 2K). Taken together, these results suggest that *Cyfip2*$^{+/-}$ mice display some of fragile X-like behaviors.

Normal steady-state expression of Cyfip2 and FMRP in *Fmr1*$^{-/y}$ and *Cyfip2*$^{+/-}$ mice, respectively

The similar behaviors of *Fmr1*$^{-/y}$ and *Cyfip2*$^{+/-}$ mice suggest that there could be shared molecular/cellular changes in the brains of these mice. We sought to identify the pathways in the hope of discovering some that might contribute to the FXS pathogenesis. As FMRP could regulate expression of hundreds of target mRNAs in brain (28) and a recent report showed altered Cyfip2

Downloaded from https://academic.oup.com/hmg/article-abstract/24/7/1813/595301
by guest
on 14 March 2018

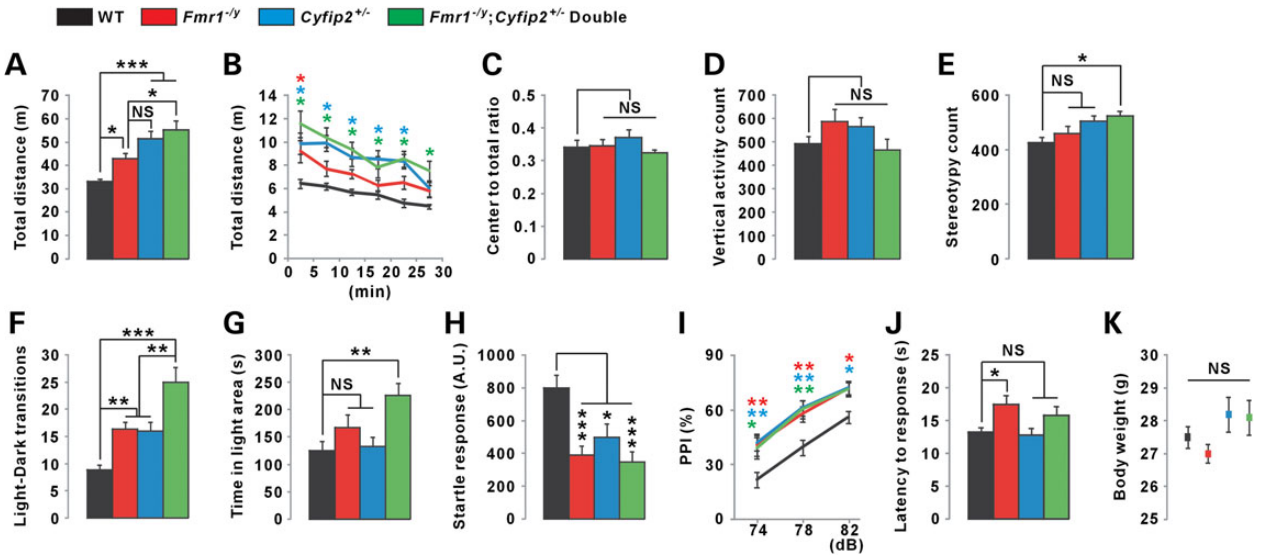

Figure 2. *Cyfip2*$^{+/-}$ mice display fragile X-like behaviors. (**A**) Hyperactivity of *Fmr1*$^{-/y}$, *Cyfip2*$^{+/-}$ and double-mutant mice in open-field test. NS, not significant. (**B**) The 5-min bin habituation curve for the open-field test. The statistical significance for each genotype is indicated by the asterisk with corresponding color. (**C** and **D**) Normal center-to-total distance ratio (C) and vertical activity count (D) of the mice during the open-field test. (**E**) Double mutant, but not *Fmr1*$^{-/y}$ or *Cyfip2*$^{+/-}$, mice showed increased stereotypy count during the open-field test. (**F**) Increased light–dark box transitions of *Fmr1*$^{-/y}$, *Cyfip2*$^{+/-}$ and double-mutant mice. (**G**) Double mutant, but not *Fmr1*$^{-/y}$ or *Cyfip2*$^{+/-}$, mice spent more time in the light area compared with WT mice. (**H** and **I**) Reduced acoustic startle response (H) and enhanced prepulse inhibition (PPI) (I) in *Fmr1*$^{-/y}$, *Cyfip2*$^{+/-}$ and double-mutant mice. (**J**) Latency to response in the hot plate test was increased in *Fmr1*$^{-/y}$ mice, but normal in *Cyfip2*$^{+/-}$ and double-mutant mice. (**K**) Normal body weights of 11-week-old *Fmr1*$^{-/y}$, *Cyfip2*$^{+/-}$ and double-mutant mice. *$P < 0.05$, **$P < 0.01$, ***$P < 0.001$. Statistical analyses for behavioral assays are in Supplementary Material, Table S2.

protein levels in the lymphocytes from FXS patients (29), we first investigated whether basal Cyfip2 and WAVE protein levels were changed in *Fmr1*$^{-/y}$ mice. We compared the protein levels in whole lysates of hippocampus and whole brain from WT, *Cyfip2*$^{+/-}$ and *Fmr1*$^{-/y}$ mice (8 weeks old). Consistent with our previous result (Fig. 1F), Cyfip2 and WAVE levels were decreased in *Cyfip2*$^{+/-}$ mice (Fig. 3A). However, these proteins were not altered in *Fmr1*$^{-/y}$ mice (Fig. 3A). We also prepared hippocampal and cortical synaptosome from *Fmr1*$^{-/y}$ mice (8 weeks old) and found that Cyfip2 and WAVE levels were normal (Fig. 3B). We observed the same result from older (12 weeks old) *Fmr1*$^{-/y}$ mice (Fig. 3C). These results suggest that, in mouse brains, loss of FMRP does not affect steady-state Cyfip2 and WAVE protein levels.

Next, we investigated the expression of FMRP in *Cyfip2*$^{+/-}$ mice. As Cyfip1/2 are direct interactors of FMRP (20), loss of Cyfip1/2 might affect the amount, distribution or function of FMRP in neurons. Indeed, in *Cyfip1*$^{+/-}$ brains, FMRP-mediated translational inhibition is altered and the protein levels of some of FMRP target mRNAs are increased (26). We first measured FMRP protein levels in hippocampal and whole-brain lysates of *Cyfip2*$^{+/-}$ mice and found that they were normal (Fig. 3A). We also investigated FMRP protein localization in cultured cortical neurons by immunostaining and found that the intensity of dendritic FMRP was normal in *Cyfip2*$^{+/-}$ neurons (Fig. 3D). Furthermore, the molecular size of major FMRP protein complex analyzed by size fractionation was normal in *Cyfip2*$^{+/-}$ cortex (Fig. 3E). Lastly, to test FMRP function, we measured the levels of amyloid precursor protein (APP) and CaMKIIα proteins in *Cyfip2*$^{+/-}$ cortex. APP and CaMKIIα are well-established FMRP targets and shown to be increased in *Fmr1*$^{-/y}$ and *Cyfip1*$^{+/-}$ brains (26). However, APP, CaMKIIα and some other synaptic protein (Homer, mGluR5, PSD-95 and Shank3) levels were normal in cortical synaptome of *Cyfip2*$^{+/-}$ mice (Fig. 3F). These results suggest that overall expression and function of FMRP are normal in *Cyfip2*$^{+/-}$ brains.

Normal hippocampal synaptic plasticity in *Cyfip2*$^{+/-}$ mice

Altered hippocampal synaptic plasticity is one of the major phenotypes in the brains of *Fmr1*-null mice (1,32), and a recent report showed enhanced hippocampal mGluR-LTD in *Cyfip1*$^{+/-}$ mice (27). Thus, we decided to test whether hippocampal synaptic plasticity was also altered in *Cyfip2*$^{+/-}$ mice, thereby contributing to the behavioral phenotypes. We first measured *N*-methyl-D-aspartate receptor (NMDAR)-dependent long-term potentiation (LTP) by extracellular field recordings at Schaffer collateral–CA1 pyramidal synapses. We did not find a difference in the degree of LTP formation between WT and *Cyfip2*$^{+/-}$ mice (Fig. 4A). Next, we measured mGluR-dependent LTD formation induced by paired-pulse low-frequency stimulation (PP-LFS) in the presence of NMDAR antagonist D-APV and found that it was normal in *Cyfip2*$^{+/-}$ hippocampus (Fig. 4B). Finally, we tested the effect of cycloheximide, an inhibitor of protein synthesis, on mGluR-LTD. Unlike in WT mice, hippocampal mGluR-LTD in *Fmr1*-null mice is not blocked by cycloheximide (9). In *Cyfip2*$^{+/-}$ mice, however, we found that cycloheximide completely blocked mGluR-LTD (Fig. 4C). Synaptic input–output relationship and paired-pulse facilitation ratio were also normal in *Cyfip2*$^{+/-}$ hippocampus (Fig. 4D and E). Taken together, these results suggest normal hippocampal synaptic plasticity of *Cyfip2*$^{+/-}$ mice. Therefore, altered hippocampal synaptic plasticity is not the mechanism that could account for the similar behavioral phenotypes between *Fmr1*$^{-/y}$ and *Cyfip2*$^{+/-}$ mice.

Abnormal cortical dendritic spines in *Cyfip2*$^{+/-}$ mice

Next, we turned our attention to the dendritic spines of *Cyfip2*$^{+/-}$ mice. We reasoned that reduced expression of Cyfip2 could affect the function of WRC and downstream actin polymerization, which will lead to changes in actin-rich dendritic spines. Supporting this hypothesis, abnormal actin polymerization and

Downloaded from https://academic.oup.com/hmg/article-abstract/24/7/1813/595301
by guest
on 14 March 2018

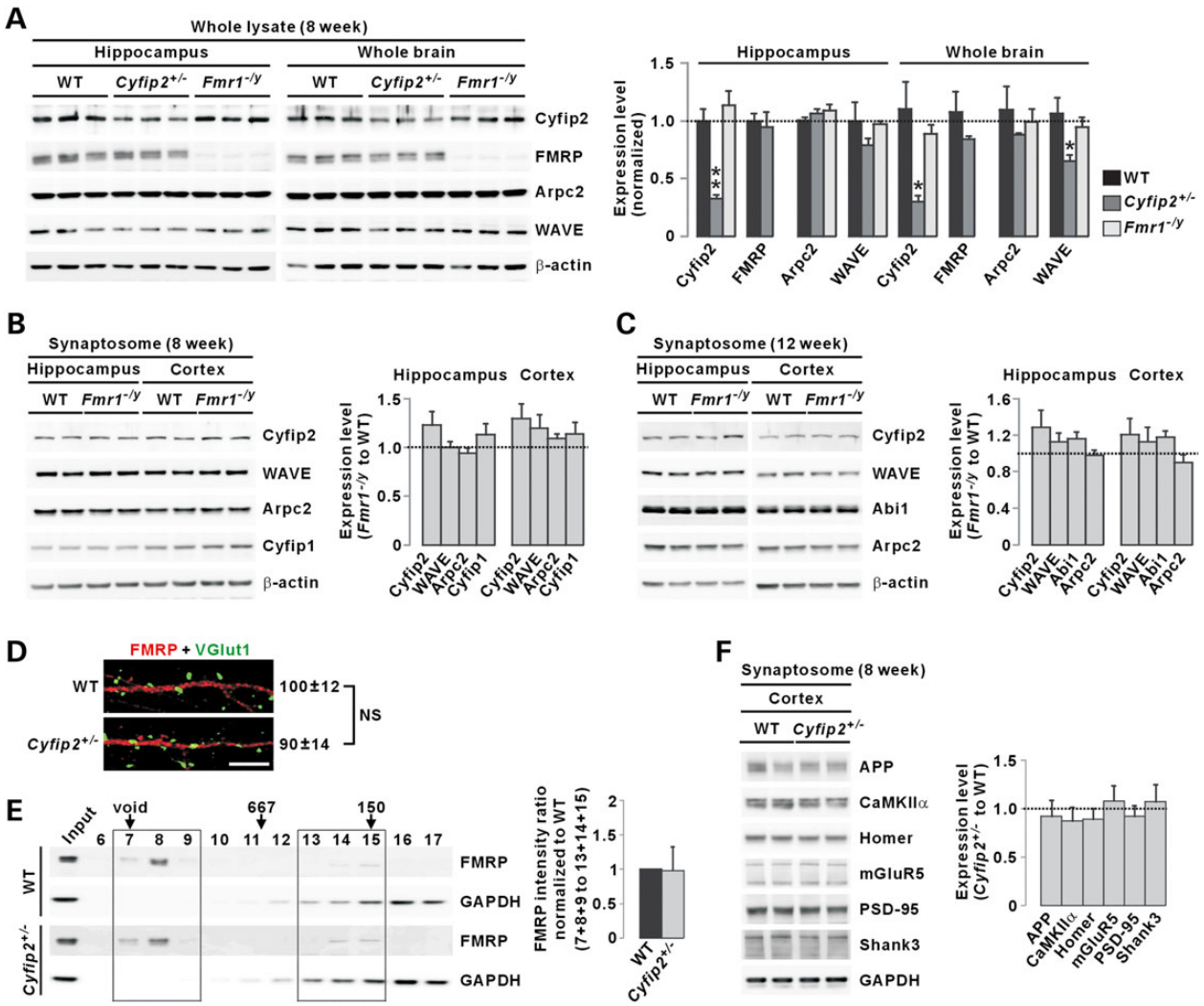

Figure 3. Steady-state expression of Cyfip2 and FMRP are normal in *Fmr1*$^{-/y}$ and *Cyfip2*$^{+/-}$ mice, respectively. (**A**) Representative western blots and quantification show that Cyfip2 and WAVE levels are decreased in hippocampal or whole brain lysates of 8-week-old *Cyfip2*$^{+/-}$ mice, but normal in *Fmr1*$^{-/y}$ mice. FMRP levels are normal in *Cyfip2*$^{+/-}$ hippocampus and whole brain ($n = 5$ animals per genotype). (**B**) Normal Cyfip2 and WAVE protein levels in hippocampal and cortical synaptosome of 8-week-old *Fmr1*$^{-/y}$ mice ($n = 7$). (**C**) Normal Cyfip2 and WAVE protein levels in hippocampal and cortical synaptosome of 12-week-old *Fmr1*$^{-/y}$ mice ($n = 7$). (**D**) Normal dendritic FMRP protein intensity in cultured *Cyfip2*$^{+/-}$ cortical neurons at DIV 14. VGlut1 is an excitatory presynaptic marker. Scale bar 10 μm. The values indicate FMRP intensity normalized to WT neurons ($n = 15$, mean ± S.E.M.). NS, not significant. (**E**) Normal molecular size of major FMRP protein complex in *Cyfip2*$^{+/-}$ cortex. Fractions 6 to 17 from Superose 6 gel purification were analyzed by western blot. The arrows indicate fractions of void, 667 and 150 kDa of calibrations. FMRP band intensity ratio of fractions 7, 8 and 9 to 13, 14 and 15 was measured and normalized to WT samples ($n = 3$). (**F**) Representative western blots and quantification show normal expression levels of APP, CaMKIIα and other synaptic proteins in *Cyfip2*$^{+/-}$ cortex ($n = 8$). *$P < 0.05$, **$P < 0.01$. Statistical analyses for western blot assays are in Supplementary Material, Table S1.

synaptic structures were observed in *Cyfip*-null *Drosophila* (24), and decreased number of dendritic spines was reported in *Wave*-1-null mice (33). We performed Golgi staining with 12-week-old WT and *Cyfip2*$^{+/-}$ brains to quantify the density of dendritic protrusions (filopodia, thin and mature spines) of apical dendrites in hippocampal CA1 and cortical layer II/III pyramidal neurons. For CA1 neurons, no significant difference in the protrusion density between WT and *Cyfip2*$^{+/-}$ mice was identified (Fig. 5A). Interestingly, for cortical neurons, numbers of mature spines and total protrusions were increased in *Cyfip2*$^{+/-}$ mice compared with WT mice (Fig. 5B).

Based on this finding, we investigated whether the changes in dendritic protrusions could account in part for the enhancement of some of fragile X-like behaviors in *Fmr1*$^{-/y}$; *Cyfip2*$^{+/-}$ double-mutant mice compared with *Fmr1*$^{-/y}$ mice (Fig. 2A and F). We performed Golgi staining and measured the density of dendritic protrusions in 10-week-old WT, *Fmr1*$^{-/y}$ and *Fmr1*$^{-/y}$; *Cyfip2*$^{+/-}$ double-mutant mice. As reported previously (11,18,34), both hippocampal and cortical neurons of *Fmr1*$^{-/y}$ mice showed increased density of thin (immature) spines compared with WT mice (Fig. 5C and D). Moreover, the number of mature spines was decreased in *Fmr1*$^{-/y}$ hippocampus (Fig. 5C). In the hippocampus of double-mutant mice, there was no further change of dendritic protrusions compared with *Fmr1*$^{-/y}$ mice (Fig. 5C). However, in the cortex of double-mutant mice, the densities of total protrusions and thin spines were further increased compared with *Fmr1*$^{-/y}$ mice (Fig. 5D). This cortex-specific enhancement of the dendritic spine phenotype in double-mutant mice is consistent with the region-specific dendritic spine change in *Cyfip2*$^{+/-}$ mice (Fig. 5A and B).

Downloaded from https://academic.oup.com/hmg/article-abstract/24/7/1813/595301
by guest
on 14 March 2018

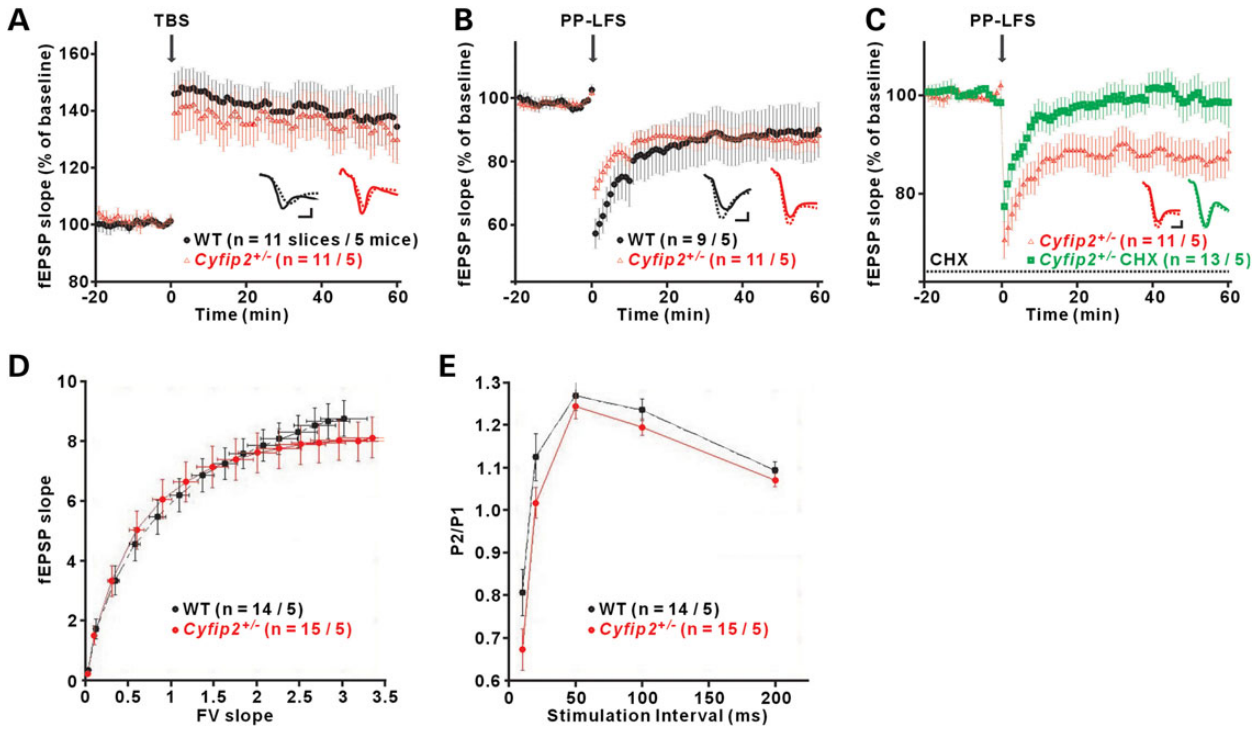

Figure 4. Normal hippocampal synaptic plasticity in *Cyfip2*$^{+/-}$ mice. (**A**) NMDAR-dependent hippocampal LTP is normal in Schaffer collateral–CA1 synapses of *Cyfip2*$^{+/-}$ mice. Numbers of slices and animals used for the experiment are indicated. Representative EPSP traces recorded at last 2 min of before (dotted line) and after (solid line) stimulation (arrow) are shown. Scale bar 2 ms, 1 mV. TBS, theta burst stimulation. (**B**) Paired-pulse low-frequency stimulation (PP-LFS)-induced hippocampal mGluR-LTD is normal in *Cyfip2*$^{+/-}$ mice. (**C**) Cycloheximide (CHX, 60 μM, dotted line) blocks PP-LFS-induced hippocampal mGluR-LTD in *Cyfip2*$^{+/-}$ mice. (**D**) Normal input–output relationship in *Cyfip2*$^{+/-}$ hippocampus. (**E**) Normal paired-pulse facilitation ratio in *Cyfip2*$^{+/-}$ hippocampus.

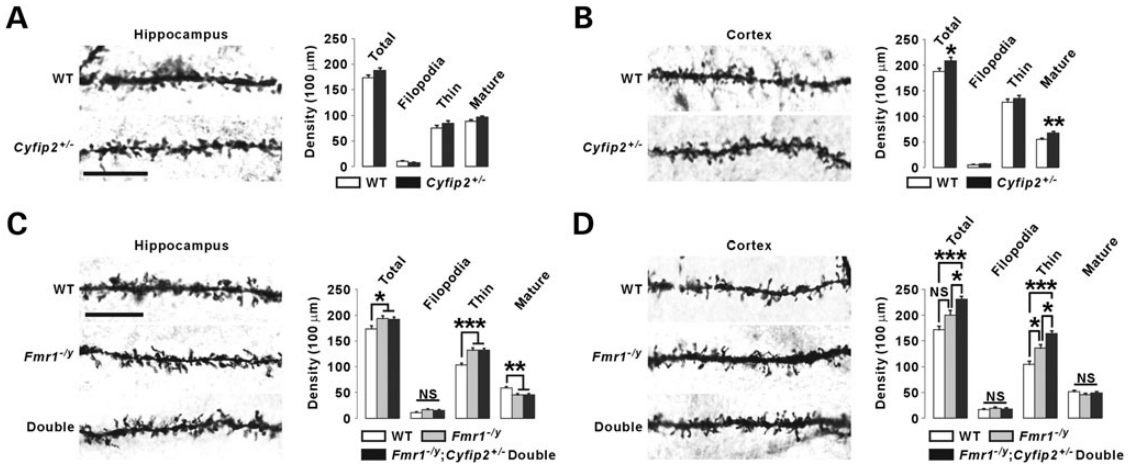

Figure 5. Abnormal cortical dendritic spines in *Cyfip2*$^{+/-}$ mice and aggravation of the *Fmr1*$^{-/y}$ cortical dendritic spine phenotype in *Fmr1*$^{-/y}$;*Cyfip2*$^{+/-}$ double-mutant mice. (**A**) Representative Golgi staining images and quantification show normal dendritic protrusions in hippocampal CA1 pyramidal neurons of *Cyfip2*$^{+/-}$ mice ($n = 43$–46 neurons from 3 animals per genotype). Scale bar 10 μm. (**B**) Increased density of mature spines and total protrusions in cortical layer II/III pyramidal neurons of *Cyfip2*$^{+/-}$ mice ($n = 33$–34). (**C**) Increased density of total protrusions and thin spines but decreased density of mature spines in hippocampal CA1 pyramidal neurons of *Fmr1*$^{-/y}$ and double-mutant mice ($n = 32$–36). NS, not significant. Scale bar 10 μm. (**D**) The densities of total protrusions and thin spines of cortical layer II/III pyramidal neurons are further increased in double-mutant mice compared with *Fmr1*$^{-/y}$ mice ($n = 44$–46). $^{*}P < 0.05$, $^{**}P < 0.01$, $^{***}P < 0.001$. Statistical analyses for dendritic protrusions are in Supplementary Material, Table S3.

mGluR-induced dendritic spine regulation and Cyfip2 expression are impaired in *Fmr1*$^{-/y}$ and *Cyfip2*$^{+/-}$ neurons

In addition to the dendritic spine changes at basal state, some forms of activity-induced regulation of dendritic spines are altered in *Fmr1*-null neurons (35). For example, mGluR agonist-induced elongation of spines of layer II/III cortical neurons is defective in early postnatal *Fmr1*-null mice (36). To determine whether Cyfip2, as a downstream target of FMRP, is required for mGluR-induced regulation of dendritic spines, we examined changes of dendritic protrusions in WT, *Fmr1*$^{-/y}$ and *Cyfip2*$^{+/-}$ neurons upon

Downloaded from https://academic.oup.com/hmg/article-abstract/24/7/1813/595301
by guest
on 14 March 2018

mGluR activation. We treated cultured cortical neurons of days *in vitro* (DIV) 14 with mGluR agonist DHPG (100 μM, 30 min). We found that treatment of DHPG decreased the number of mature spines and increased the average length of dendritic protrusions in WT neurons (Fig. 6A). In contrast, the same treatment did not affect dendritic protrusions in either *Fmr1*$^{-/y}$ or *Cyfip2*$^{+/-}$ neurons (Fig. 6B and C). These data suggest that *Fmr1*$^{-/y}$ and *Cyfip2*$^{+/-}$ cortical neurons have similar defect in mGluR-induced spine regulation. To explore the underlying mechanism, we first tested the effect of cycloheximide. We found that pre-incubation of cycloheximide (60 μM, 30 min) blocked the DHPG-induced spine change in cultured WT cortical neurons, suggesting that new protein synthesis was required for the process (Fig. 6D). This is consistent with the previous finding in hippocampal slice cultures where inhibition of protein synthesis blocked DHPG-induced spine change (37).

Based on this result, we came back to the previous report that *Cyfip2* mRNA is a high-ranked FMRP target in mouse brain (28). mGluR activation induces translation of FMRP-associated mRNAs, and this process is impaired in *Fmr1*-null neurons (38,39). We hypothesized that mGluR activation could induce translation of *Cyfip2* mRNA, which then might mediate mGluR-induced spine regulation. If our hypothesis is correct, this process should be impaired in both *Fmr1*$^{-/y}$ and *Cyfip2*$^{+/-}$ neurons, owing to absence of the regulator or target mRNA, respectively (Fig. 6E). We first tested whether DHPG treatment can increase Cyfip2 proteins in cultured WT cortical neurons. Indeed, 20 min of DHPG incubation increased Cyfip2 proteins by 40% (Fig. 6F). As positive controls, APP and PSD-95 proteins were also increased by DHPG treatment (Fig. 6F) (39,40). Pre-incubation of cycloheximide blocked the DHPG-induced Cyfip2 increase, suggesting its dependence on protein synthesis (Fig. 6F). Importantly, DHPG treatment in either *Fmr1*$^{-/y}$ or *Cyfip2*$^{+/-}$ cortical neurons did not significantly change Cyfip2 protein levels (Fig. 6G and H). WAVE protein levels were not altered in any treatment conditions (Fig. 6F–H). Taken together, these results suggest that mGluR activation increases Cyfip2 proteins through its mRNA translation and that a defect in this process might account in part for the abnormal mGluR-induced spine regulation in *Fmr1*$^{-/y}$ and *Cyfip2*$^{+/-}$ cortical neurons.

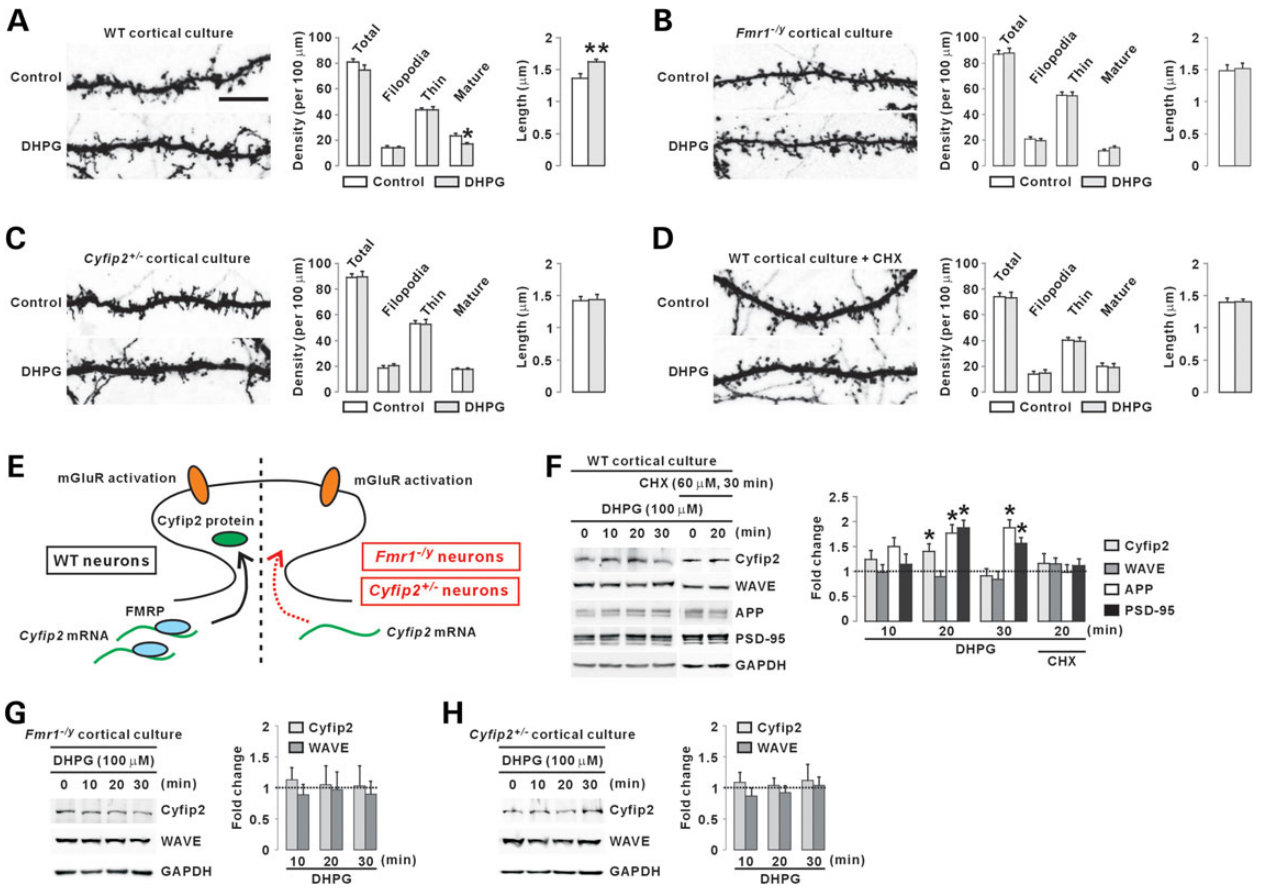

Figure 6. mGluR-induced dendritic spine change and Cyfip2 expression are defective in *Fmr1*$^{-/y}$ and *Cyfip2*$^{+/-}$ cortical neurons. (**A**) DHPG (100 μM, 30 min) treatment decreases mature spine density and increases average protrusion length in cultured WT cortical neurons ($n = 28$–32 neurons per condition). Neurons were transfected with EGFP-expressing plasmids and immunostained with GFP antibody. Scale bar 10 μm. (**B** and **C**) DHPG treatment fails to change dendritic spines in *Fmr1*$^{-/y}$ ($n = 24$) (B) and *Cyfip2*$^{+/-}$ cortical neurons ($n = 21$-30) (C). (**D**) Pre-incubation of cycloheximide (CHX; 60 μM, 30 min) blocks DHPG-induced spine change in WT cortical neurons ($n = 20$–21). (**E**) Diagram shows the hypothesis that mGluR activation induces FMRP-dependent translation of *Cyfip2* mRNA, which could be required for mGluR-induced regulation of dendritic spines. In *Fmr1*$^{-/y}$ or *Cyfip2*$^{+/-}$ neurons, mGluR activation fails to induce Cyfip2 expression. (**F**) 20 min of incubation of DHPG (100 μM) increases Cyfip2 proteins in cultured WT cortical neurons, which is blocked by pre-incubation of cycloheximide (60 μM, 30 min). Cyfip2 levels are not significantly changed by 10 or 30 min of DHPG incubation. WAVE levels are not affected by DHPG treatment. APP and PSD-95 are positive controls for DHPG treatment ($n = 8$). (**G** and **H**) DHPG treatment fails to increase Cyfip2 protein levels in cultured *Fmr1*$^{-/y}$ (G) and *Cyfip2*$^{+/-}$ (H) cortical neurons ($n = 4$–6). *$P < 0.05$, **$P < 0.01$. Statistical analyses for western blot assays and dendritic protrusions are in Supplementary Material, Table S1 and S3, respectively.

Downloaded from https://academic.oup.com/hmg/article-abstract/24/7/1813/595301
by guest
on 14 March 2018

Discussion

Despite recent identification of hundreds of FMRP target mRNAs in brain, the proteins causing the respective neurobehavioral and anatomical phenotypes of FXS are poorly defined (7). The behavioral and dendritic spine phenotypes in *Cyfip2*$^{+/-}$ and *Fmr1*$^{-/y}$; *Cyfip2*$^{+/-}$ mice, together with mGluR-induced translation of *Cyfip2* mRNA that is impaired in *Fmr1*$^{-/y}$ neurons, suggest that Cyfip2 mediates, in part, the neuropathogenesis of FXS. By examining multiple potential mechanisms, we could reveal cortical dendritic spines as the common pathway regulated by FMRP and Cyfip2.

The cortical dendritic spines of *Cyfip2*$^{+/-}$ neurons were abnormal in both basal and mGluR-induced conditions. In basal condition, *Cyfip2*$^{+/-}$ cortical neurons showed increased numbers of mature and total dendritic spines. Notably, this is the opposite phenotype to *Wave-1* RNAi-transfected or null neurons (33,41), suggesting that the net WAVE activity could be enhanced in *Cyfip2*$^{+/-}$ cortical neurons in spite of reduced WAVE protein levels. This is consistent with the enhanced filamentous actin assembly in *Cyfip*-null *Drosophila* where WAVE proteins are also reduced (24). The neuronal phenotype of *Cyfip*-null *Drosophila* is rescued by deleting one copy of *SCAR* gene (the *Drosophila* homolog of *Wave*), strongly supporting enhanced WAVE activity after loss of Cyfip (24). This is further supported by another study showing that the pentameric WRC is inactive whereas WAVE-Abi-HSPC300 trimer (without Cyfip and Nap) is active *in vitro* (42). Together, these results suggest that, without Cyfip2, WAVE is first activated because of the free VCA domain and then is degraded owing to reduced stability (24,25). This activation is sufficient to drive the increased number of mature dendritic spines.

In contrast to the cortex, both WAVE protein levels and dendritic spines were normal in *Cyfip2*$^{+/-}$ hippocampus. One possibility is that Cyfip1 is preferentially used to assemble WRC in hippocampus; thus, haploinsufficiency of *Cyfip2* does not affect hippocampal WAVE activity and stability. We also found that hippocampal mGluR-LTD was normal in *Cyfip2*$^{+/-}$ mice, whereas it is enhanced in *Cyfip1*$^{+/-}$ mice (27). This result suggests region-specific differential roles of Cyfip1 and Cyfip2 in brain function and suggests that *Cyfip1* and *Cyfip2* double-mutant mice might have broader fragile X-like phenotypes than each of single-mutant mice.

At this point, it is not easy to understand whether the increased mature spines and WAVE activity in *Cyfip2*$^{+/-}$ cortex directly cause the fragile X-like behaviors in the mice, because *Fmr1*$^{-/y}$ brains have more immature spines and normal WAVE protein levels. Nevertheless, Rac1 pathway including its downstream effectors, such as WAVE and PAK, could be overactivated in *Fmr1*$^{-/y}$ brains, and this could contribute to the behavioral phenotypes, as inhibition of PAK rescues both cortical dendritic spine phenotype and some of the behaviors in *Fmr1*$^{-/y}$ mice (18,19). Accordingly, the aggravation of some of behavioral and cortical dendritic spine phenotypes in *Fmr1*$^{-/y}$;*Cyfip2*$^{+/-}$ double-mutant mice compared with *Fmr1*$^{-/y}$ mice could be explained by the additive or synergistic activation of Rac1 pathway in cortical neurons. Testing the effect of genetic or pharmacological inhibition of WAVE activity in *Fmr1*$^{-/y}$ mice on their behavioral phenotypes might provide further evidence for the pathogenic role of Rac1 pathway in FXS.

In addition to the basal condition, we found that mGluR-induced regulation of dendritic spines was defective in both *Fmr1*$^{-/y}$ and *Cyfip2*$^{+/-}$ cortical neurons. New protein synthesis is required for the mGluR-induced spine regulation, as cycloheximide blocked this process. Indeed, we found that mGluR activation induced mRNA translation-dependent increase of Cyfip2 in WT cortical neurons, which was also impaired in *Fmr1*$^{-/y}$ and *Cyfip2*$^{+/-}$ neurons. Interestingly, the steady-state level of Cyfip2 was normal in *Fmr1*-null brains. Therefore, FMRP could be more involved in mGluR-induced expression of Cyfip2 than its basal expression in neurons. Similarly, normal basal, but defective mGluR-induced expression of PSD-95 was observed in *Fmr1*-null cortical neurons (39). These results, together with a previous study identifying *Cyfip2* mRNA as a high-ranked FMRP target in brain (28), suggest that FMRP could be directly associated with *Cyfip2* mRNA to regulate its mGluR-induced translation and that Cyfip2 expression might be required for the mGluR-induced dendritic spine change.

As we observed the increase of Cyfip2 proteins from whole neuronal lysates, it remains to be determined whether the mGluR-induced Cyfip2 synthesis occurred in neuronal dendrites. Notably, a recent study showed dendritic localization of *Cyfip2* mRNAs (43). Thus, it might be possible that FMRP regulates mGluR-induced dendritic transport and local translation of *Cyfip2* mRNAs, as it does for other target mRNAs (38). Visualization of both *Cyfip2* mRNAs and proteins in neuronal dendrites before and after mGluR activation will be necessary to answer these questions. It is also not clear yet how acute Cyfip2 expression could contribute to the mGluR-induced spine regulation. One possible hypothesis is that the newly synthesized Cyfip2 interferes with the binding of Rac1-GTP to preexisting Cyfip2 in WRC. This will block the activation of WAVE in WRC and downstream Arp2/3 complex, thereby leading to decrease number of mature spines and increase protrusion length. Further investigation of the functional relationship between Cyfip2 and FMRP, both at the protein and mRNA levels, and on their roles in regulating actin cytoskeleton will help us better understand this process and its implication to FXS.

Materials and Methods

Animals

Cyfip2$^{+/-}$ mice were generated by injecting the ES cell (Cyfip2$^{tm1(KOMP)Vlcg}$) purchased from UCDAVIS KOMP Repository. *Cyfip2*$^{+/-}$ mice were maintained in C57BL/6J background. *Fmr1*-null mice in C57BL/6J background were provided by Dr David Nelson (Baylor College of Medicine). The mice were housed 3–5 per cage in a room with 12-h light and dark schedule. All experiments were performed with 2- to 3-month-old male mice, unless otherwise specified. All experimental procedures were reviewed and approved by the Institutional Animal Care and Use Committee for Baylor College of Medicine.

Biochemistry and antibodies

Mouse brain whole lysates, synaptosome and PSDI fraction were prepared as described previously (44). Briefly, mouse brains were homogenized in buffered sucrose (0.32 M sucrose, 4 mM HEPES, 1 mM $MgCl_2$, 0.5 mM $CaCl_2$, pH 7.3) with freshly added protease inhibitors (Roche; 04693159001). The homogenate was centrifuged at 900*g* for 10 min. The resulting supernatant was centrifuged again at 12 000*g* for 15 min (the supernatant after this centrifuge is S2). The pellet was resuspended in buffered sucrose and centrifuged at 13 000*g* for 15 min (the resulting pellet is P2; crude synaptosome). To obtain PSDI fractions, the synaptosomal fraction was extracted with Triton X-100.

To analyze the molecular size of FMRP protein complex, mouse cortex was homogenized in extraction buffer (50 mM

Downloaded from https://academic.oup.com/hmg/article-abstract/24/7/1813/595301
by guest
on 14 March 2018

Tris pH 8.0, 75 mM NaCl, 0.5% Triton X-100, 30 mM EDTA plus protease and phosphatase inhibitor cocktail) and centrifuged at 16 000*g* for 10 min. The supernatant was transferred into new tube and centrifuged one more time. The resulting supernatant was spun over a 0.45-µm microfuge spin filter (Corning) at 3 300*g* for 1 min and applied to a Superose 6 10/300 GL column (GE Healthcare) using an Akta Purifier 10 system (GE Healthcare). The column was run with a flow rate of 0.3 ml/min and 1 ml/fraction. The column was calibrated with thyroglobulin at 667 kDa, alcohol dehydrogenase at 150 kDa and cytochrome-C at 12.3 kDa (Sigma). Antibodies used for western blots are Abi1 (Sigma–Aldrich; A5106), APP (Millipore; MAB348), Arpc2 (Millipore; 07-227), β-actin (Abcam; ab20272), CaMKIIα (Abcam; ab22609), Cyfip1 (Abcam; ab108220), Cyfip2 (Abcam; ab95969), FMRP (Cell Signaling Technology; 4317), GAPDH (Millipore; CB1001), mGluR5 (Millipore; AB5675), PSD-95 (NeuroMab; 75-028), Shank3 (Santa Cruz; H-160) and WAVE1 (NeuroMab; 75-048). Western blot images were acquired by LAS 4000 (GE Healthcare) and quantified using ImageJ.

RNA extraction and quantitative real-time reverse transcription PCR

Total RNA was extracted from 50 to 70 mg of each brain region using a miRNeasy minikit (Qiagen) according to the manufacturer's instruction. One microgram of DNase-treated total RNA was used to synthesize cDNA using Quantitect Reverse Transcription Kit (Qiagen). Quantitative real-time reverse transcription PCR (qRT-PCR) experiments were performed using the CFX96 Touch Real-Time PCR Detection System (Bio-Rad Laboratories) with PerfeCta SYBR Green FastMix, ROX (Quanta Biosciences). To unambiguously distinguish spliced cDNA from genomic DNA contamination, we designed specific exon primers across introns using Primer3 v.0.4.0 (45) as follows:

Cyfip1 forward 5′ GGTTATGGCAGGAAGTTTGC 3′
reverse 5′ GATCGTGGCTCCCTGATTT 3′
Cyfip2 forward 5′ AGATGTACCTGACGCCCAGT 3′
reverse 5′ TGACATTTCCGTCCATCAGA 3′
Wave-1 forward 5′ CGATGTGTGTGAGCAACCTC 3′
reverse 5′ TCAGCCCTTCCTTACCATCA 3′
Gapdh forward 5′ GGCATTGCTCTCAATGACAA 3′
reverse 5′ CCCTGTTGCTGTAGCCGTAT 3′

The results were analyzed using the comparative Ct method normalized against the housekeeping gene *Gapdh* as described previously (46).

Behavioral assays

Behavioral assays were performed with 8- to 10-week-old animals as described previously (47). Before each test, mice were habituated in the test room at least for 30 min. For open-field test, mice were habituated in the test room (600 lux, 60 dB white noise) and placed in the center of a clear, open Plexiglass chamber (40 × 40 × 30 cm). The activities were measured by photobeam breaks (Accuscan) for 30 min. Light–dark box assay was performed in the same test room using the box consisted of a clear Plexiglas chamber (36 × 20 × 26 cm) with an open top separated from a covered black chamber (15.5 × 20 × 26 cm) by a black partition with a small opening. The movements were measured by photobeam breaks (Accuscan) for 10 min. For acoustic startle response and prepulse inhibition, mice were placed in a test chamber (San Diego Instruments) and habituated for 5 min with 70 dB background white noise. Eight trial types (no stimulus, a 40-ms 120 dB sound as the startle stimulus, and three different prepulse sounds (20 ms 74, 78, 82 dB) either alone or 100 ms before the startle stimulus) were presented in pseudo-random order with six times per each trial type. The interval between each trial type was 10–20 s. The maximum startle amplitude during the 65-ms period following the onset of the startle stimulus was used to calculate percentage prepulse inhibition. Hot plate test was performed using a Plexiglass chamber enclosing a hot plate at 55 ± 0.1°C. The latency to hind limb nociceptive response (jumping, shaking or licking the hind paw) was measured.

Electrophysiology

Mice were deeply anesthetized with isofluorane, followed by decapitation. The brain was removed and quickly immersed in ice-cold cutting solution containing (in mM): 110 sucrose, 60 NaCl, 3 KCl, 1.25 NaH_2PO_4, 28 $NaHCO_3$, 0.5 $CaCl_2$, 7 $MgCl_2$ and 5 glucose. Transverse hippocampal slices of 400 µm of thickness were prepared with a Vibratome. Next, cortical tissue was removed and hippocampal slices were recovered in an equal mix of cutting solution and artificial cerebrospinal fluid (ACSF) containing (in mM): 125 NaCl, 1.25 NaH_2PO_4, 2.5 KCl, 25 $NaHCO_3$, 2 $CaCl_2$, 1 $MgCl_2$ and 15 glucose at room temperature for 10 to 20 min before transferring into interface recording chambers (Fine Science Tools). Slices were perfused (1.5 ml per min) with ACSF saturated with 95% O_2/5% CO_2 at 31°C.

Stimulation electrode was placed at the striatum radiatum to stimulate the Schaffer collateral pathway, and fEPSPs of CA1 neurons were recorded with an ACSF-filled glass recording electrode (1–3 MΩ). Electrophysiological traces were amplified with AC-coupled amplifier (model 1800; A-M Systems), digitized using a Digidata 1320A and acquired with pClamp software (Molecular Devices). The input–output relationship was used to estimate the general synaptic transmission properties of this pathway. Specifically, the rising slope of the fEPSP evoked by 100 µs pulses over various stimulus intensities (1 to 10 V) was measured. The stimulation intensity that evoked a fEPSP that had a slope of 30–35% of the maximum fEPSP slope determined by the input–output was used for measuring paired-pulse ratio and LTP formation. For LTD formation, the stimulation strength that gave 50–60% of the maximal fEPSP slope was used. Recordings that did not exhibit stable fEPSP slope during the first 20 min of recording were excluded.

Paired-pulse ratios were assessed via systematic variation of the inter-stimulus interval (10, 20, 50, 100 and 200 ms). LTP formation was induced by a theta burst stimulation (TBS) paradigm consisting five bursts of four pulses at 100 Hz separated by 200 ms (4-month-old mice). To monitor LTP formation, the fEPSPs were recorded every 20 s for 20 min before and 60 min after TBS. The magnitude of potentiation was determined by measuring the rising slope of the fEPSP (for summary, traces were averaged for every 1-min interval). LTD formation was induced with a paired-pulse low-frequency stimulation paradigm consisting 1 Hz of paired stimuli separated by 50 ms for 20 min. 50 µM D-AP5 (Tocris) was included in ACSF for LTD experiments. For LTD, 5- to 7-week-old mice were used. 60 µM cycloheximide (Sigma) were used to examine the contribution of protein synthesis for LTD formation.

Golgi staining

Standard Golgi-Cox impregnation using the FD Rapid Golgistain kit (NeuroTechnologies) was performed with serial sagittal brain sections (50 µm). Images of dendritic spines on the secondary branches (apical dendrites of hippocampal CA1 and cortical

Downloaded from https://academic.oup.com/hmg/article-abstract/24/7/1813/595301
by guest
on 14 March 2018

layer II/III pyramidal neurons) were acquired by LSM710 (Zeiss) confocal microscope under DIC mode. Dendritic filopodia were defined as protrusions without head and having a length at least twice the width. Mature spines were defined as protrusions with heads and having a width greater than length. The rest of protrusions with heads were categorized as thin spines. The images were quantified in blind manner using ImageJ.

Neuron culture, transfection and immunostaining

Neuron culture, transfection and immunostaining were performed as described previously (47). Neurons were transfected with pEGFP-C1 (empty vector) at days *in vitro* (DIV) 10, and fixed and immunostained at DIV 14. Antibodies used for immunostaining are FMRP (Millipore; MAB2160), GFP (Abcam; ab290) and VGlut1 (Synaptic Systems; 135 302). (RS)-3,5-Dihydroxyphenylglycine (DHPG; Tocris) (100 μM) was applied for 30 min before fixation. The images were quantified in blind manner using ImageJ. To measure DHPG-induced protein expression, cultured neurons (DIV 14) incubated with DHPG (100 μM) were directly lysed with 2× Laemmli sample buffer for western blot analysis. Cycloheximide (60 μM) was added to the media 30 min before and during DHPG treatment.

Statistical analysis

All data acquisition and analysis were carried out blinded to genotype. Statistical significance was determined by Student's *t*-test or ANOVA with Tukey's *post hoc* analysis using GraphPad Prism version 6. All data are presented as mean ± S.E.M. $^{*}P < 0.05$; $^{**}P < 0.01$; $^{***}P < 0.001$.

Supplemental Material

Supplementary Material is available at *HMG* online.

Acknowledgements

We thank G. Schuster for generating *Cyfip2*-mutant mice.

Conflict of Interest statement. None declared.

Funding

This work was supported by The Howard Hughes Medical Institute (to H.Y.Z.); and the Baylor Intellectual and Developmental Disabilities Research Center (P30HD024064) confocal, electrophysiology and mouse neurobehavioral cores.

References

1. Bhakar, A.L., Dolen, G. and Bear, M.F. (2012) The pathophysiology of fragile X (and what it teaches us about synapses). *Annu. Rev. Neurosci.*, **35**, 417–443.
2. Santoro, M.R., Bray, S.M. and Warren, S.T. (2012) Molecular mechanisms of fragile X syndrome: a twenty-year perspective. *Annu. Rev. Pathol.*, **7**, 219–245.
3. Pieretti, M., Zhang, F.P., Fu, Y.H., Warren, S.T., Oostra, B.A., Caskey, C.T. and Nelson, D.L. (1991) Absence of expression of the FMR-1 gene in fragile X syndrome. *Cell*, **66**, 817–822.
4. Verkerk, A.J., Pieretti, M., Sutcliffe, J.S., Fu, Y.H., Kuhl, D.P., Pizzuti, A., Reiner, O., Richards, S., Victoria, M.F., Zhang, F.P. *et al.* (1991) Identification of a gene (FMR-1) containing a CGG repeat coincident with a breakpoint cluster region exhibiting length variation in fragile X syndrome. *Cell*, **65**, 905–914.
5. Heitz, D., Rousseau, F., Devys, D., Saccone, S., Abderrahim, H., Le Paslier, D., Cohen, D., Vincent, A., Toniolo, D., Della Valle, G. *et al.* (1991) Isolation of sequences that span the fragile X and identification of a fragile X-related CpG island. *Science*, **251**, 1236–1239.
6. Fu, Y.H., Kuhl, D.P., Pizzuti, A., Pieretti, M., Sutcliffe, J.S., Richards, S., Verkerk, A.J., Holden, J.J., Fenwick, R.G. Jr., Warren, S.T. *et al.* (1991) Variation of the CGG repeat at the fragile X site results in genetic instability: resolution of the Sherman paradox. *Cell*, **67**, 1047–1058.
7. Darnell, J.C. and Klann, E. (2013) The translation of translational control by FMRP: therapeutic targets for FXS. *Nat. Neurosci.*, **16**, 1530–1536.
8. Huber, K.M., Gallagher, S.M., Warren, S.T. and Bear, M.F. (2002) Altered synaptic plasticity in a mouse model of fragile X mental retardation. *Proc. Natl Acad. Sci. USA*, **99**, 7746–7750.
9. Nosyreva, E.D. and Huber, K.M. (2006) Metabotropic receptor-dependent long-term depression persists in the absence of protein synthesis in the mouse model of fragile X syndrome. *J. Neurophysiol.*, **95**, 3291–3295.
10. Krueger, D.D. and Bear, M.F. (2011) Toward fulfilling the promise of molecular medicine in fragile X syndrome. *Annu. Rev. Med.*, **62**, 411–429.
11. Comery, T.A., Harris, J.B., Willems, P.J., Oostra, B.A., Irwin, S.A., Weiler, I.J. and Greenough, W.T. (1997) Abnormal dendritic spines in fragile X knockout mice: maturation and pruning deficits. *Proc. Natl Acad. Sci. USA*, **94**, 5401–5404.
12. Irwin, S.A., Patel, B., Idupulapati, M., Harris, J.B., Crisostomo, R.A., Larsen, B.P., Kooy, F., Willems, P.J., Cras, P., Kozlowski, P.B. *et al.* (2001) Abnormal dendritic spine characteristics in the temporal and visual cortices of patients with fragile-X syndrome: a quantitative examination. *Am. J. Med. Genet.*, **98**, 161–167.
13. Hering, H. and Sheng, M. (2001) Dendritic spines: structure, dynamics and regulation. *Nat. Rev. Neurosci.*, **2**, 880–888.
14. Nakayama, A.Y., Harms, M.B. and Luo, L. (2000) Small GTPases Rac and Rho in the maintenance of dendritic spines and branches in hippocampal pyramidal neurons. *J. Neurosci.*, **20**, 5329–5338.
15. Castets, M., Schaeffer, C., Bechara, E., Schenck, A., Khandjian, E.W., Luche, S., Moine, H., Rabilloud, T., Mandel, J.L. and Bardoni, B. (2005) FMRP interferes with the Rac1 pathway and controls actin cytoskeleton dynamics in murine fibroblasts. *Hum. Mol. Genet.*, **14**, 835–844.
16. Chen, L.Y., Rex, C.S., Babayan, A.H., Kramar, E.A., Lynch, G., Gall, C.M. and Lauterborn, J.C. (2010) Physiological activation of synaptic Rac>PAK (p-21 activated kinase) signaling is defective in a mouse model of fragile X syndrome. *J. Neurosci.*, **30**, 10977–10984.
17. Schenck, A., Bardoni, B., Langmann, C., Harden, N., Mandel, J.L. and Giangrande, A. (2003) CYFIP/Sra-1 controls neuronal connectivity in Drosophila and links the Rac1 GTPase pathway to the fragile X protein. *Neuron*, **38**, 887–898.
18. Hayashi, M.L., Rao, B.S., Seo, J.S., Choi, H.S., Dolan, B.M., Choi, S.Y., Chattarji, S. and Tonegawa, S. (2007) Inhibition of p21-activated kinase rescues symptoms of fragile X syndrome in mice. *Proc. Natl Acad. Sci. USA*, **104**, 11489–11494.
19. Dolan, B.M., Duron, S.G., Campbell, D.A., Vollrath, B., Shankaranarayana Rao, B.S., Ko, H.Y., Lin, G.G., Govindarajan, A., Choi, S.Y. and Tonegawa, S. (2013) Rescue of fragile X syndrome phenotypes in Fmr1 KO mice by the small-molecule PAK inhibitor FRAX486. *Proc. Natl Acad. Sci. USA*, **110**, 5671–5676.
20. Schenck, A., Bardoni, B., Moro, A., Bagni, C. and Mandel, J.L. (2001) A highly conserved protein family interacting with

Downloaded from https://academic.oup.com/hmg/article-abstract/24/7/1813/595301
by guest
on 14 March 2018

the fragile X mental retardation protein (FMRP) and displaying selective interactions with FMRP-related proteins FXR1P and FXR2P. *Proc. Natl Acad. Sci. USA*, **98**, 8844–8849.
21. Takenawa, T. and Suetsugu, S. (2007) The WASP-WAVE protein network: connecting the membrane to the cytoskeleton. *Nat. Rev. Mol. Cell Biol.*, **8**, 37–48.
22. Chen, Z., Borek, D., Padrick, S.B., Gomez, T.S., Metlagel, Z., Ismail, A.M., Umetani, J., Billadeau, D.D., Otwinowski, Z. and Rosen, M.K. (2010) Structure and control of the actin regulatory WAVE complex. *Nature*, **468**, 533–538.
23. Kunda, P., Craig, G., Dominguez, V. and Baum, B. (2003) Abi, Sra1, and Kette control the stability and localization of SCAR/WAVE to regulate the formation of actin-based protrusions. *Curr. Biol.*, **13**, 1867–1875.
24. Zhao, L., Wang, D., Wang, Q., Rodal, A.A. and Zhang, Y.Q. (2013) Drosophila cyfip regulates synaptic development and endocytosis by suppressing filamentous actin assembly. *PLoS Genet.*, **9**, e1003450.
25. Abekhoukh, S. and Bardoni, B. (2014) CYFIP family proteins between autism and intellectual disability: links with Fragile X syndrome. *Front. Cell. Neurosci.*, **8**, 81.
26. Napoli, I., Mercaldo, V., Boyl, P.P., Eleuteri, B., Zalfa, F., De Rubeis, S., Di Marino, D., Mohr, E., Massimi, M., Falconi, M. *et al.* (2008) The fragile X syndrome protein represses activity-dependent translation through CYFIP1, a new 4E-BP. *Cell*, **134**, 1042–1054.
27. Bozdagi, O., Sakurai, T., Dorr, N., Pilorge, M., Takahashi, N. and Buxbaum, J.D. (2012) Haploinsufficiency of Cyfip1 produces fragile X-like phenotypes in mice. *PLoS One*, **7**, e42422.
28. Darnell, J.C., Van Driesche, S.J., Zhang, C., Hung, K.Y., Mele, A., Fraser, C.E., Stone, E.F., Chen, C., Fak, J.J., Chi, S.W. *et al.* (2011) FMRP stalls ribosomal translocation on mRNAs linked to synaptic function and autism. *Cell*, **146**, 247–261.
29. Hoeffer, C.A., Sanchez, E., Hagerman, R.J., Mu, Y., Nguyen, D.V., Wong, H., Whelan, A.M., Zukin, R.S., Klann, E. and Tassone, F. (2012) Altered mTOR signaling and enhanced CYFIP2 expression levels in subjects with fragile X syndrome. *Genes. Brain Behav.*, **11**, 332–341.
30. Kumar, V., Kim, K., Joseph, C., Kourrich, S., Yoo, S.H., Huang, H.C., Vitaterna, M.H., de Villena, F.P., Churchill, G., Bonci, A. *et al.* (2013) C57BL/6N mutation in Cytoplasmic FMRP interacting protein 2 regulates cocaine response. *Science*, **342**, 1508–1512.
31. Spencer, C.M., Alekseyenko, O., Hamilton, S.M., Thomas, A.M., Serysheva, E., Yuva-Paylor, L.A. and Paylor, R. (2011) Modifying behavioral phenotypes in Fmr1KO mice: genetic background differences reveal autistic-like responses. *Autism Res.*, **4**, 40–56.
32. Sidorov, M.S., Auerbach, B.D. and Bear, M.F. (2013) Fragile X mental retardation protein and synaptic plasticity. *Mol. Brain*, **6**, 15.
33. Soderling, S.H., Guire, E.S., Kaech, S., White, J., Zhang, F., Schutz, K., Langeberg, L.K., Banker, G., Raber, J. and Scott, J.D. (2007) A WAVE-1 and WRP signaling complex regulates spine density, synaptic plasticity, and memory. *J. Neurosci.*, **27**, 355–365.
34. Bhattacharya, A., Kaphzan, H., Alvarez-Dieppa, A.C., Murphy, J.P., Pierre, P. and Klann, E. (2012) Genetic removal of p70 S6 kinase 1 corrects molecular, synaptic, and behavioral phenotypes in fragile X syndrome mice. *Neuron*, **76**, 325–337.
35. Portera-Cailliau, C. (2012) Which comes first in fragile X syndrome, dendritic spine dysgenesis or defects in circuit plasticity? *Neuroscientist*, **18**, 28–44.
36. Cruz-Martin, A., Crespo, M. and Portera-Cailliau, C. (2012) Glutamate induces the elongation of early dendritic protrusions via mGluRs in wild type mice, but not in fragile X mice. *PLoS One*, **7**, e32446.
37. Vanderklish, P.W. and Edelman, G.M. (2002) Dendritic spines elongate after stimulation of group 1 metabotropic glutamate receptors in cultured hippocampal neurons. *Proc. Natl Acad. Sci. USA*, **99**, 1639–1644.
38. Bassell, G.J. and Warren, S.T. (2008) Fragile X syndrome: loss of local mRNA regulation alters synaptic development and function. *Neuron*, **60**, 201–214.
39. Todd, P.K., Mack, K.J. and Malter, J.S. (2003) The fragile X mental retardation protein is required for type-I metabotropic glutamate receptor-dependent translation of PSD-95. *Proc. Natl Acad. Sci. USA*, **100**, 14374–14378.
40. Westmark, C.J. and Malter, J.S. (2007) FMRP mediates mGluR5-dependent translation of amyloid precursor protein. *PLoS Biol.*, **5**, e52.
41. Kim, Y., Sung, J.Y., Ceglia, I., Lee, K.W., Ahn, J.H., Halford, J.M., Kim, A.M., Kwak, S.P., Park, J.B., Ho Ryu, S. *et al.* (2006) Phosphorylation of WAVE1 regulates actin polymerization and dendritic spine morphology. *Nature*, **442**, 814–817.
42. Padrick, S.B., Cheng, H.C., Ismail, A.M., Panchal, S.C., Doolittle, L.K., Kim, S., Skehan, B.M., Umetani, J., Brautigam, C.A., Leong, J.M. *et al.* (2008) Hierarchical regulation of WASP/WAVE proteins. *Mol. Cell*, **32**, 426–438.
43. Cajigas, I.J., Tushev, G., Will, T.J., tom Dieck, S., Fuerst, N. and Schuman, E.M. (2012) The local transcriptome in the synaptic neuropil revealed by deep sequencing and high-resolution imaging. *Neuron*, **74**, 453–466.
44. Han, K., Kim, M.H., Seeburg, D., Seo, J., Verpelli, C., Han, S., Chung, H.S., Ko, J., Lee, H.W., Kim, K. *et al.* (2009) Regulated RalBP1 binding to RalA and PSD-95 controls AMPA receptor endocytosis and LTD. *PLoS Biol.*, **7**, e1000187.
45. Koressaar, T. and Remm, M. (2007) Enhancements and modifications of primer design program Primer3. *Bioinformatics*, **23**, 1289–1291.
46. Han, K., Gennarino, V.A., Lee, Y., Pang, K., Hashimoto-Torii, K., Choufani, S., Raju, C.S., Oldham, M.C., Weksberg, R., Rakic, P. *et al.* (2013) Human-specific regulation of MeCP2 levels in fetal brains by microRNA miR-483-5p. *Genes Dev.*, **27**, 485–490.
47. Han, K., Holder, J.L. Jr., Schaaf, C.P., Lu, H., Chen, H., Kang, H., Tang, J., Wu, Z., Hao, S., Cheung, S.W. *et al.* (2013) SHANK3 overexpression causes manic-like behaviour with unique pharmacogenetic properties. *Nature*, **503**, 72–77.

Downloaded from https://academic.oup.com/hmg/article-abstract/24/7/1813/595301
by guest
on 14 March 2018